Applied Radiation and Isotopes 156 (2020) 108953

Contents lists available at ScienceDirect

Applied Radiation and Isotopes

journal homepage: http://www.elsevier.com/locate/apradiso

A novel technique for the optimization and reduction of gamma spectroscopy geometry uncertainties

Thomas Frosio *, Nabil Menaa, Philippe Bertreix, Maeva Rimlinger, Chris Theis

Radiation Protection Group, European Organization for Nuclear Research, 1211, Geneva 23, Switzerland

ARTICLE INFO

Keywords:
Gamma-spectroscopy
Uncertainty quantification
Uncertainty optimization
Geometric model
ISOCS/LabSOCS
Hotspots
Efficiency

ABSTRACT

Material activation can sometimes cause large heterogeneities in the distribution of radioactivity (hotspots). Moreover, the sample geometry parameters are not always well known. When performing gamma-spectroscopy to quantify the radionuclide inventory in activated materials, often predefined models are used to represent the sample geometry (dimensions, source-to-detector distance, material type) and their activity distribution, for efficiency calibration. This simplification causes uncertainties of the efficiency curves associated with the model and consequently, to the activity results. In this paper, we develop a new approach, based on ISOCS/LabSOCS to quantify and reduce uncertainties originating from the geometry model. The theory is described in this document and an experimental case is discussed.

1. Introduction

Gamma-spectroscopy [1](or gamma-spectrometry) techniques are non-destructive methods used without resorting to sample preparation. They are of interest for activities like waste elimination, shipping of radioactive goods, or physics experiments to quantify gamma emitting radionuclides in materials. Nowadays, tools like ISOCS (In Situ Counting Object Software (Venkataraman et al., 2003)) allow for the computation of efficiency calibrations in order to calculate activities of these samples without needing special radioactive standards for efficiency calibration. Monte-Carlo simulations require longer computing times whereas efficiency calibration curves generation with ISOCS allows constructing thousands of models in a couple of hours, depending on the complexity of the geometry. Moreover, Monte-Carlo modelling require validating the geometry model prior to using it. On the other hand, validating a Monte-Carlo model of the geometry requires the use of calibrated radioactive sources, which are not available for all users and adds both complexity and operating costs to the user processes. The added value of basing our methodology on ISOCS is the fact that it provides an a priori validated intrinsic efficiency model at the factory. Moreover, the ISOCS mathematical efficiency calibration has been widely accepted by regulatory authorities as a valid calibration method. The ISOCS gamma-spectroscopy reports present activity values and their associated uncertainties. These uncertainties take into account only the contributions that are caused by the numerical approximations related to the efficiency computation, and the uncertainties from peak area and emission intensity. However, recent studies focus on uncertainties originating from the geometry model parameters such as activity distribution (Kaminski et al., 2014), (Sima, 2017), (Sima, 2018), dimensions, material types, source to detector distance, etc (Nakazawaet al., 2010), (Venkataraman et al., 2005), (Bronsonet al., 2008). The efficiency computation is based on a geometric model of the sample and the detector. The model depends on the dimensions, relative source concentrations, positions of hotspots, layers and might sometimes carry considerable uncertainties. This aspect is less relevant for small laboratory samples but reveals itself more in large objects. As example, CERN's operates electromagnets in order to guide beam particles. These magnets can reach some tenth of tons and length of 6 m. Due to the secondary particle cascades (respectively the complex geometry), uncertainties on activity distribution (respectively dimensions and composition material) can affect the efficiency calibration curves produced with standard geometries. Similar problems arise for large containers, due to the difficulty to know the activity distribution inside with sufficient certainty. Consequently, this problem is inherent to large scale dismantling or maintenance activities of nuclear installations as well as treatment of radioactive waste from accelerator installations.

This document aims at providing a thorough theoretical basis which allows for performing a precise analysis of the involved uncertainties

* Corresponding author.
E-mail addresses: thomas.frosio@gmail.com, thomas.frosio@cern.ch (T. Frosio).

[1] Throughout this paper, the two words spectroscopy and spectrometry are used interchangeably.

https://doi.org/10.1016/j.apradiso.2019.108953
Received 12 June 2019; Received in revised form 10 October 2019; Accepted 22 October 2019
Available online 30 October 2019

and the possibility of reducing them. These uncertainties are coming from the whole knowledge we have about the samples to be analyzed (dimensions, masses, distance source-detector, activity distribution). For this purpose, a tool has been developed and contains two modules: the former quantifies the geometry uncertainties and the latter reduces them by matching spectroscopy results to identify the best-estimate model. The investigated techniques for the quantification and reduction of uncertainties are made sustainable via a software tool that we have developed. The tool is named GURU (Geometry Uncertainty Reduction Utility).

This paper covers in detail the theory of the developments made and gives a validation on three application cases.

The first part of this document targets at describing the tools that are currently used in CERN's radioanalytical laboratory for gamma-spectroscopy analyses, along with the input and output data structure. Then the second part focuses essentially on the usability of the ISOCS/IUE standard tool results to perform sensitivity analysis and uncertainty propagation to quantify the associated activities uncertainties due to the not-well known model. This first module of GURU is named Data-Analyzer. The third part details the uncertainty reduction technique using the GURU SpectroMatcher optimization module. The mathematical framework is described below. An emphasis is put on the description of the heterogeneity of the sample's activity concentration, as it is a rather complex aspect that goes beyond the current state-of-the-art treatment. The fourth part details the experimental setups used to validate the methodology developed. Finally, a "case-Study" application of the DataAnalyzer and SpectroMatcher modules of the GURU tool is performed to illustrate and validate the GURU methodology, algorithms, implementation, and results.

2. Activity calculation procedure

2.1. In Situ Counting Object Software (Isocs)

ISOCS (In Situ Counting Object Software) and LabSOCS (Laboratory Sourceless Calibration Software) (Menaaet. al., 2011) from Canberra are used at CERN laboratories for creating efficiency calibrations curves without using radioactive standards at the laboratory. The geometry description can be visualized and edited in the ISOCS/LabSOCS Geometry Composer application (See Fig. 1) which contains a visualization interface of the sample geometry.

2.2. Isocs Uncertainty Estimator (Iue)

The generation of the ISOCS/LabSOCS efficiency calibration curves is performed by the creation of a geometric model of the sample to be measured. The geometry parameters are: dimensions, materials compositions, densities, detector position and orientation, and activity distribution within the sample. These parameters are not always known with accuracy. The commercially available ISOCS Uncertainty Estimator (IUE) tool, developed by Canberra, allows the perturbation of these parameters to quantify the effect on the efficiency calibration curves. By generating a set of perturbed models, IUE generates the associated efficiency calibration curves for the sample to be measured. Consequently, uncertainty and sensitivity analysis can be done with IUE. An example of geometry parameters intervals in IUE interface is provided in Figs. 2, 3 and 4.

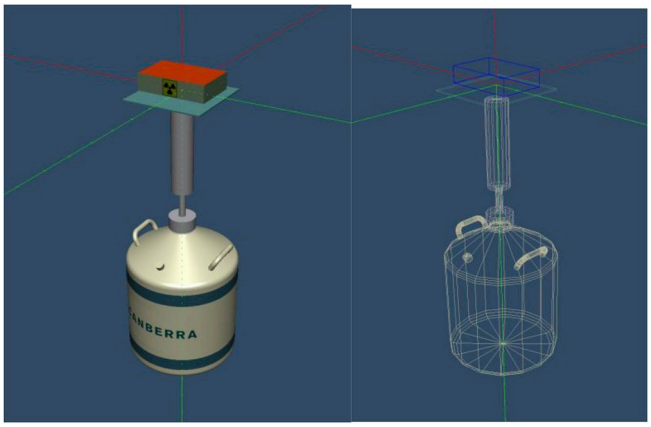

Fig. 1. Example of geometry model generated by ISOCS/LabSOCS.

2.3. Activity computation

Once all the geometry parameters are set in the Geometry Composer software, the efficiencies over a user-selected energy mesh are calculated. Then, the activity of the measured sample is given by the following Equation (1):

Equation 1. Gamma-spectroscopy activity calculation

$$A = \frac{N_s(E)}{\varepsilon(E).\Delta t} \times \frac{1}{I_\gamma(E)}$$

Where:

A is the activity of a certain radionuclide in the decay series;
$N_s(E)$ is the net peak area corresponding to energy E;
$\varepsilon(E)$ is the absolute full-energy peak efficiency corresponding to the geometric model at energy E;
$I_\gamma(E)$ is the emission intensity of photons with energy E;
Δt is time for collecting the spectrum of the sample.

2.4. Isocs and Iue files

ISOCS and IUE (Bosko et al., 2011), (Spillane et al., 2010), (Bronson et al., 1997), (Venkataraman et al., 1999) generate different files that are of interest for the quantification and reduction of uncertainties. All the information about the geometry and efficiencies is stored in these files.

A unique ISOCS calculation produces the. GIS and. ECC files. They respectively contain the geometry of the model (dimensions, material, activity distribution …) and the corresponding efficiencies at different energies.

A multiple ISOCS simulation triggered via the IUE interface generates two other files: the. UGS and the. UEC files. The. UGS file contains all the modelled geometries that are simulated with input parameter perturbations configured by the user. The. UEC file contains the associated efficiency calibrations. In addition, the sample can present an heterogeneous distribution of the activities. Hence, different hotspots can be located inside the model. In the latter case, ISOCS is limited to a single hotspot in the model in the Complex Box template. Consequently, to overcome this limitation, multiple ISOCS calculations are needed depending on the number of hotspots requested by the user. A dedicated section concerning the treatment of hotspots is detailed later in the document. While IUE allows modelling multiple hotspots within the sample, it is limited to a single concentration for all hotspots.

3. Quantification of models uncertainties

The sensitivity analysis plays an important role in order to quantify the most impacting parameters of the sample model on the calculated efficiencies and the associated activities. It is the first step in quantifying the uncertainties as it allows for excluding the parameters whose effects are negligible. As calculations can be very time consuming, reducing the system to a lower dimensional phase-space is very time effective.

In addition, the sensitivity analysis allows for quantifying the efficiency variation trends. For instance, a linear perturbation of a model

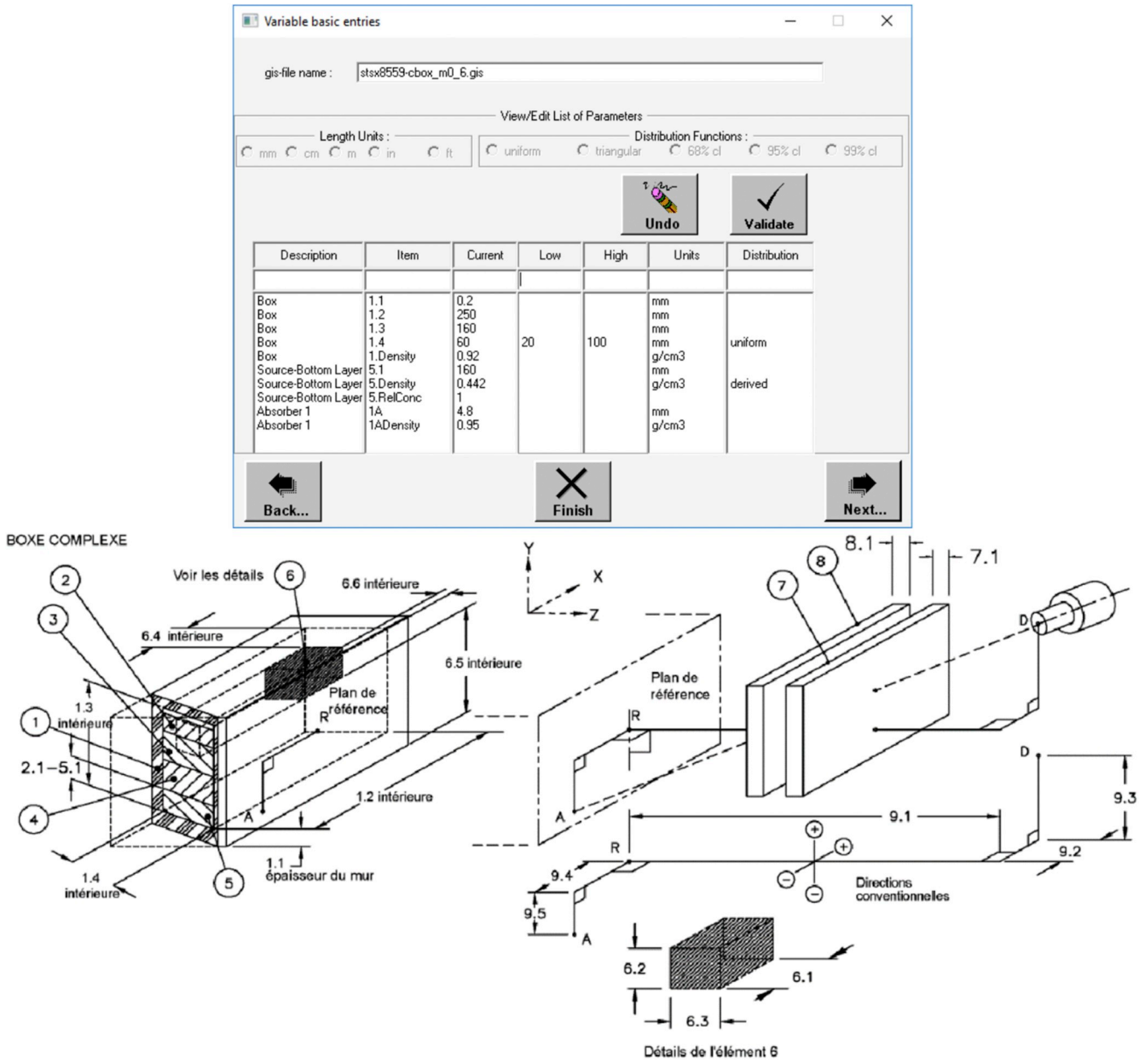

Fig. 2. Typical IUE data input screen. Parameters are entered here to describe the amount and type of variation for the model.

parameter could lead to a linear perturbation of the efficiency. This trends study could turn out to be necessary and useful as one could generate sensitivity databases from which the user could deduce the efficiency variation due to a parameter variation without the need to perform further ISOCS calculations.

Once the most sensitive parameters are identified, the user could generate the uncertainty model by varying all relevant parameters simultaneously.

When gamma-spectroscopy measurements are performed on samples, the knowledge of the geometry description (Ilieet al., 2013), including dimensions, position with respect to the detector, material composition, hotspots or relative source concentration is often not well known, especially for the two last parameters. We propose a method to identify the model that is most compliant with the available data, based on the combination of different gamma spectroscopy results. The software tool GURU has been developed to organize the different data extracted from ISOCS/IUE. The DataAnalyzer module is described in this section and the SpectroMatcher module is described in section 3.

In all what follows, we only focus on the "complex box" template (Fig. 2) from ISOCS for simplicity and practicality reasons, as consequence GURU works only with the "complex box" template. Furthermore, in our workflow, this is the most often used template as we often use boxes as enclosing geometry. The analysis could be extended to cylindrical geometries in a second step to describe more situations.

A summary of the sequential use of GURU is presented in appendix 1, Fig. 14.

Other tools and methods can be found in the literature to quantify uncertainties of gamma-spectroscopy measurements (Ceccatelliet al., 2017), (Belgya, 2014).

3.1. *Sensitivity analysis by perturbing one-factor-at-a-time (Oat)*

The sensitivity analysis aims to determine the parameters of the model contributing the most to the variability of outputs of the model.

Let's assume we have a starting model of the sample. We refer to this initial model as the reference model. The reference model is based on a

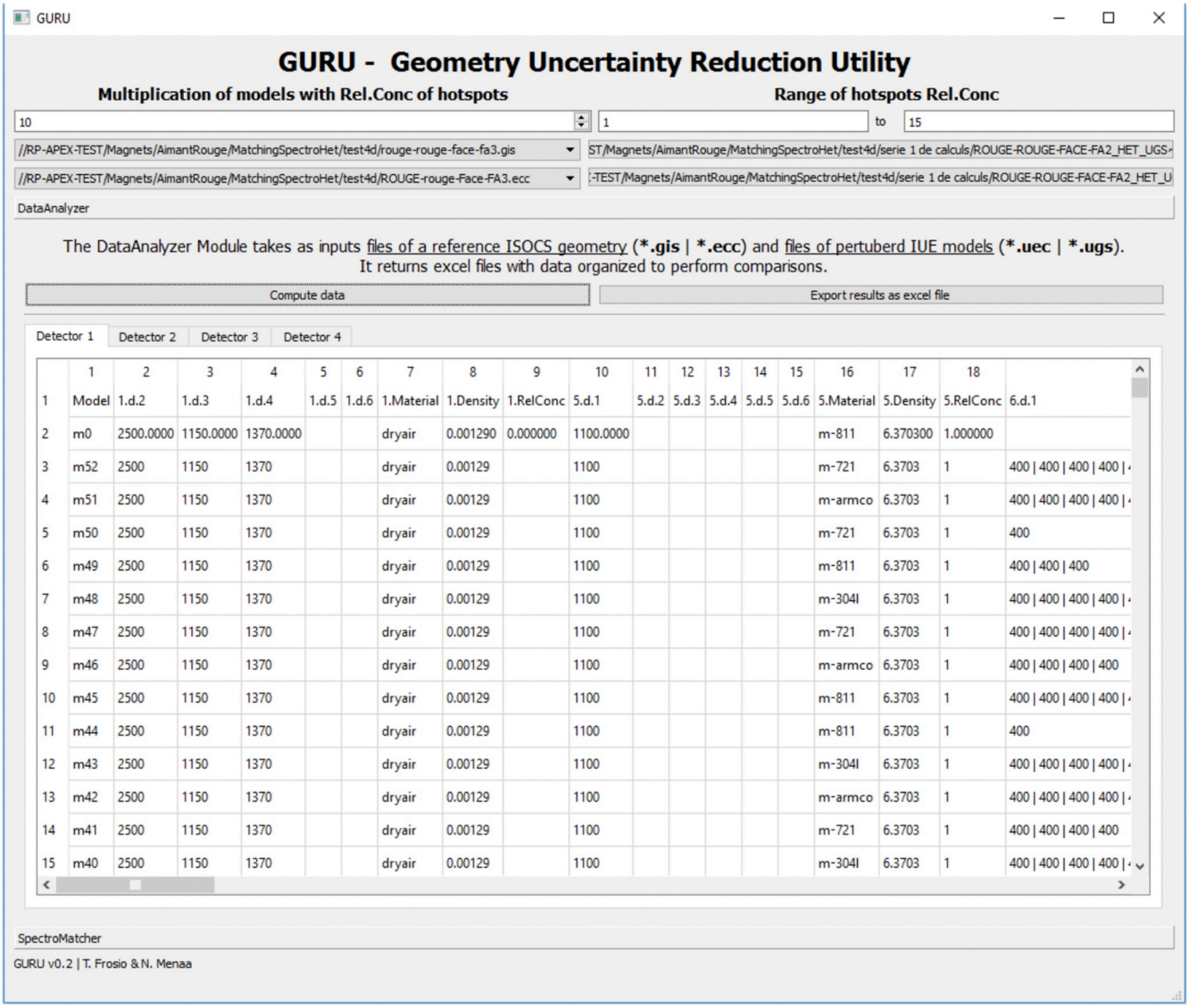

	1	2	3	4	5	6	7	8	9	10	11	12	13	14	15	16	17	18	
1	Model	1.d.2	1.d.3	1.d.4	1.d.5	1.d.6	1.Material	1.Density	1.RelConc	5.d.1	5.d.2	5.d.3	5.d.4	5.d.5	5.d.6	5.Material	5.Density	5.RelConc	6.d.1
2	m0	2500.0000	1150.0000	1370.0000			dryair	0.001290	0.000000	1100.0000						m-811	6.370300	1.000000	
3	m52	2500	1150	1370			dryair	0.00129		1100						m-721	6.3703	1	400 | 400 | 400 | 400 |
4	m51	2500	1150	1370			dryair	0.00129		1100						m-armco	6.3703	1	400 | 400 | 400 | 400 |
5	m50	2500	1150	1370			dryair	0.00129		1100						m-721	6.3703	1	400
6	m49	2500	1150	1370			dryair	0.00129		1100						m-811	6.3703	1	400 | 400 | 400
7	m48	2500	1150	1370			dryair	0.00129		1100						m-304l	6.3703	1	400 | 400 | 400 | 400 |
8	m47	2500	1150	1370			dryair	0.00129		1100						m-721	6.3703	1	400 | 400 | 400 | 400 |
9	m46	2500	1150	1370			dryair	0.00129		1100						m-armco	6.3703	1	400 | 400 | 400 | 400
10	m45	2500	1150	1370			dryair	0.00129		1100						m-811	6.3703	1	400 | 400 | 400 | 400 |
11	m44	2500	1150	1370			dryair	0.00129		1100						m-811	6.3703	1	400
12	m43	2500	1150	1370			dryair	0.00129		1100						m-304l	6.3703	1	400 | 400 | 400 | 400 |
13	m42	2500	1150	1370			dryair	0.00129		1100						m-armco	6.3703	1	400 | 400 | 400 | 400 |
14	m41	2500	1150	1370			dryair	0.00129		1100						m-721	6.3703	1	400 | 400 | 400 | 400
15	m40	2500	1150	1370			dryair	0.00129		1100						m-304l	6.3703	1	400 | 400 | 400 | 400 |

Fig. 3. Snapshot of the GURU DataAnalyzer screen. It allows for associating the geometry parameters to the IUE/ISOCS efficiency results.

set of geometry parameters to which we associate corresponding uncertainties. In order to establish the variation intervals of the efficiencies, one needs to sample the parameter variations using a specific probability distribution. This distribution could be uniform if only the interval limits are known, Gaussian if the unknown parameter is normally distributed around the initial value (GUM and Evaluation of Measurement Data, 2008a) … etc.

After computation of. UGS,.UEC files from IUE representing the perturbed models and. GIS,.ECC files from ISOCS representing the reference model, we can calculate the variation of activity for a variation of the geometric parameter according to Equation (2):

Equation 2. Variation of efficiency and activities for perturbed models compared to the reference. Top equation: absolute perturbations. Bottom equation: relative perturbations

$$\varepsilon_{model\ i}(\vec{X}) - \varepsilon_{model\ ref}(\vec{X}) = \partial\varepsilon\varepsilon_{model\ i}(\vec{X}) \qquad \frac{\varepsilon_{model\ ref}(\vec{X})}{\varepsilon_{model\ ref}(\vec{X})} - 1 = \partial\varepsilon_{\%}$$

Where:

$\varepsilon_{model\ i}$ is the efficiency using "model i" at energy E,
$\varepsilon_{model\ ref}$ is the efficiency using the reference model at energy E,
$\vec{X}$ denotes the vector of variable model parameters (X_0, …X_i, ….X_n)

The values $\partial\varepsilon$ and $\partial\varepsilon_{\%}$ in Equation (2) represent the absolute and relative efficiency variations that correspond to the variation of one or multiple parameters. By dividing this quantity by the absolute or relative variation of a model parameter X_i perturbed, ∂X_i we get the relative sensitivity S^{ε}_{Xi} of ε to Xi (supposed to be linearly dependent) as shown in Equation (3):

Equation 3. Sensitivity of efficiency to model parameters

$$S^{\varepsilon}_{Xi} = \frac{\partial\varepsilon}{\partial Xi}$$

The sensitivity is an indicator of the dependency of the output on the input. When this value is high, it means that the X_i parameter impacts the efficiency considerably. However, this is not the only value of interest as, uncertainties can be high for a parameter having low impact, leading to high perturbations of efficiency results.

Hence, in what follows we will focus on the relative change of the

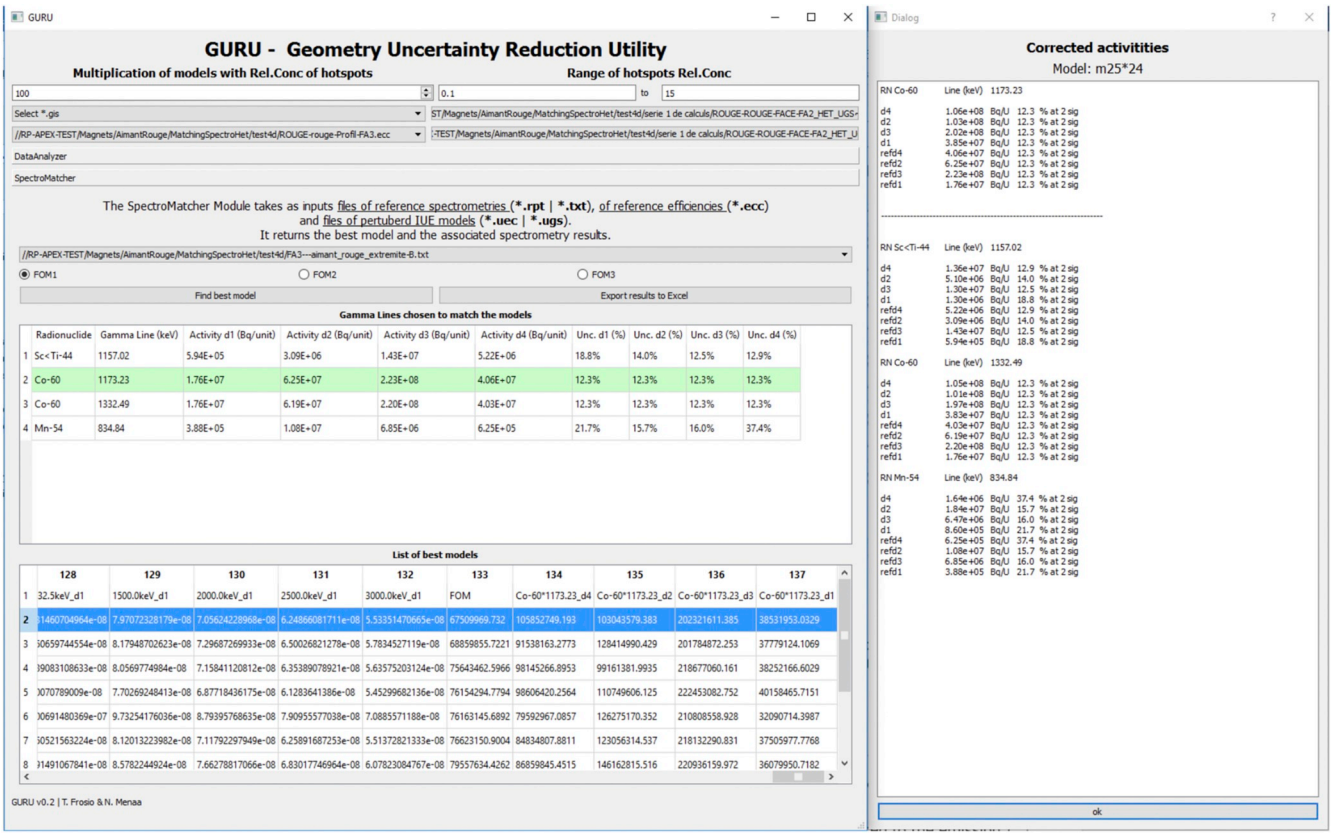

Fig. 4. A view of the SpectroMatcher to select the best geometric model of ISOCS for computing activity.

efficiency curve as a results of uncertainties propagations.

3.2. Uncertainty propagation formalism

The uncertainty propagation equation is presented in Equation (4) (GUM and Evaluation of Measurement Data, 2008b):

Equation 4. Sensitivity of efficiency to model parameters

$$\sigma^2(\varepsilon) = \sum_i \sum_j \frac{\partial \varepsilon}{\partial X_i} \frac{\partial \varepsilon}{\partial X_j} \sigma(X_i)\sigma(X_j) r_{i,j} = S_X^{\varepsilon} \boldsymbol{M} S_X^{\varepsilon\, T}$$

Where $\frac{\partial \varepsilon}{\partial X_i}$ represents the sensitivity of the efficiency to the parameter. X_i

$\sigma(X_i)$ is denoted as the uncertainty of the parameter X_i
$r_{i,j}$ is the Pearson correlation between X_i and X_j

Or in a matrix form:

$$S_X^{\varepsilon} = \begin{pmatrix} \frac{\partial \varepsilon}{\partial X_1} \\ \cdots \\ \frac{\partial \varepsilon}{\partial X_i} \end{pmatrix}$$ is the sensitivity vector

$$\boldsymbol{M} = \begin{bmatrix} \sigma^2(X_1) & \cdots & \sigma(X_1)\sigma(X_j) r_{1,j} \\ \vdots & \ddots & \vdots \\ \sigma(X_i)\sigma(X_1) r_{i,1} & \cdots & \sigma^2(X_i) \end{bmatrix}$$ is the variance-covariance matrix

This propagation law allows for quantifying the uncertainty of the efficiency: $\sigma(\varepsilon)$.

3.3. Combination of Iue results

In order to quantify uncertainties and sensitivities, GURU offers a framework of data analysis originating from IUE.

The output of IUE is a collection of model efficiencies and parameters in four separate files: ".GIS,.ECC,.UGS, and. UEC". In order to fully exploit the results, a DataAnalyzer framework tool named "GURU" is needed to associate the model parameters to the efficiency values. The tool is currently used in-house and will be integrated into our workflow for specific applications. A snapshot of the tool is shown in Fig. 3.

The IUE data and ISOCS/LabSOCS files are treated in GURU and combined in order to associate parameter perturbations with efficiency perturbations. Three sets of data are calculated for each detector:

- Association of efficiency to each model,
- Absolute sensitivities, and
- Relative sensitivities.

The user is able to use this collection of data to compute and visualize the uncertainties by exporting the results in an excel file.

4. Model optimization to reduce geometry uncertainties

4.1. Matching/optimization of gamma spectroscopy results

The GURU SpectroMatcher (see Fig. 4) module makes use of the following two constraints:

- The *multiple gamma spectroscopy scans, performed at different locations of a sample, should yield the same expected value of the total activity.* This is referred to as the multi-count consistency. That can be used

with systems based on multiple detectors such as in (Zhanget al., 2017).

- The activities calculated for each gamma emission line of the same radionuclide should be consistent. This is referred to as the Line Activity Consistency or "LAC".

These features are exploited by GURU to perform an optimization (Bronson, 1997) in order to determine the best set of geometry models that fulfil the above requirements.

When IUE is used by modelling different detectors, we can correlate the efficiencies of these different detectors together. Then, knowing the activity values from each detector for a reference model, we can correct these activities by the ratio of efficiencies as shown in the next Equation (5) derived from Equation (1):

Equation 5. Activity correction from efficiency ratio

$$\forall i,j,k, \quad A_i^k(j) = \frac{\varepsilon_{ref}^k(E)}{\varepsilon_i^k(E)} A_{ref}^k(j)$$

Where $A_i^k(j)$ represents the calculated activity for the radionuclide associated to the emission j in the model i with the detector k,

$\varepsilon_{ref}^k(E)$ represents the reference efficiency at energy E of emission j from the detector k

$\varepsilon_i^k(E)$ represents the efficiency of model i at energy E of emission j from the detector k

$A_{ref}^k(j)$ is the activity calculated with the reference model from detector k and emission j

Using Equation (5), a set of activities can be calculated for each radionuclide emission, in each model and detector.

Then using the line and count consistencies, we match the activities between the different detectors. To this end, we construct a Figure Of Merit (FOM) as follows for each gamma emission$j$ and model i:

Equation 6. Partial FOM of a gamma line emission

$$FOM_i(j) = \sum_{k=1}^{K} \left(A_i^k(j) - < A_i(j) > \right)^2$$

Where $< A_i(j) >$ is the average over the K detectors of the activity for the gamma emission j in the model: $< A_i(j) > = \sum_{k=1}^{K} \frac{A_i^k(j)}{K}$,

$A_i^k(j)$ represents the activity calculated for the radionuclide associated to the emission j in the model i with the detector k.

For each gamma emission, a rank is assigned from 1 to "n" for all models based on their performance, where n is the total number of models (e.g., 50). The best model in each approach is assigned #1, the second best - #2, and so on. Then for each model i the composite total FOM (denoted as $Rank_i$) is obtained by adding the individual ranks assigned based on each of the methods j selected to be used during optimization:

Finally, the total $Rank_i$ for a model i is calculated for each model i as:

Equation 7. Total rank of a model

$$Rank_i = \sum_{j=0}^{J} Rank_i^j$$

Where J represents the number of common gamma emission lines found for each detector.

The model with the minimum $Rank_i$ is considered as the best model. The user needs to select the gamma lines to perform the optimization. These gamma lines are proposed by the software only if the reference activity results include them in all detector counts. Note that Equation (6) is one of the possible FOM expressions for ranking the geometry models. GURU offers the possibility to select other FOMs that take into account the activity uncertainties, for example. Nevertheless, we considered in this study the FOM described in equation (6). The effect of the various FOMs expressions is the subject of future studies.

4.2. Case of multiple hotspots

In the following we focus on the specific case of the "complex box" with one homogeneous source layer filling the entire container and multiple hotspots. In this specific case, ISOCS can only model one hotspot. However, IUE allows for the computation of a random number of hotspots in the box with different geometries, positions and materials. When this kind of computations are requested from IUE, for n hotspots asked by the user, IUE creates $2n$ calculations corresponding to different representations of the model. Then, these computations are combined by GURU to construct the efficiency of the model containing n hotspots. In the next part of this document, we detail a novel formalism of combining the hotspots. A verification and validation of this new method is performed on 2 examples.

4.2.1. Special case: 2 hotspots formalism

We first consider a model with two hotspots for the sake of simplicity and then extend this theory to n hotspots. The IUE computation gives a first set of efficiencies, which corresponds to hotspots h_1 and h_2 calculated with their relative source concentration. However, the total model (denoted as "total") is the sum of h_1 and h_2 with a complex box whose hotspots have relative source concentration of 0. This geometry is denoted #. The scheme of reconstruction is detailed in Fig. 5.

The efficiency $\varepsilon(E)$ at energy E is the ratio of number of counts in the full energy peak corresponding to energy E denoted $N(E)$ with respect to the number of photons emitted with energy E by the source $C(E)$. In what follows, we drop the dependency in energy (Equation (8)):

Equation 8. Efficiency depending on detector counts and source emissions

$$\varepsilon = \frac{N}{C}$$

From Equation (8), we derive Equation (9) by simply replacing the number of counts in the full-energy peak and source emission in the volume denoted as "total" by the ones from the volumes at the right hand side of the equality. Equation (9) gives the efficiency of the total model:

Equation 9. Efficiency depending on the detector counts and source emissions

$$\varepsilon_{total} = \frac{N_{total}}{C_{total}} = \frac{N_\# + N_{h1} + N_{h2}}{C_\# + C_{h1} + C_{h2}} = \frac{1}{C_\# + C_{h1} + C_{h2}} \left(\frac{N_\# C_\#}{C_\#} + \frac{N_{h1} C_{h1}}{C_{h1}} + \frac{N_{h2} C_{h2}}{C_{h2}} \right)$$

Then using the efficiency ε of each individual model, we get Equation (10):

Equation 10. Efficiency of the total model containing the two hotspots

$$\varepsilon_{total} = \frac{\varepsilon_\# C_\# + \varepsilon_{h1} C_{h1} + \varepsilon_{h2} C_{h2}}{C_\# + C_{h1} + C_{h2}}$$

Where $\frac{C_i}{m_i} = R_i$ with R_i being the relative source concentration of i and m_i

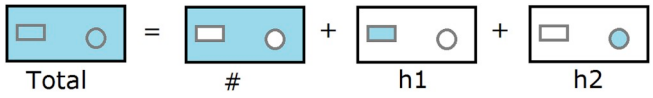

Fig. 5. Combination of hotspots geometries with the geometry containing no hotspots. Blue color represents the volume inside the sample which has a relative source concentration different from 0. Grey shapes (square and circle) represent two distinct hotspots and black shape represent the complex box. (For interpretation of the references to color in this figure legend, the reader is referred to the Web version of this article.)

the mass of i.

However, efficiency of model # is not given by IUE. Instead, IUE gives efficiencies of two additional models denoted t_1 and t_2. These models correspond to the sum of # with a hotspot whose relative source concentration contribution is not taken into account ($R_{\#} = R_{h1} = R_{h2}$). Note that the attenuation effects within the sample is taken into account as the individual efficiency calibrations are calculated using ISOCS (t_1, $t_2 h_1$, h_2). Those calculations include the impacts due to the material type and densities of the sample. Then the efficiency of # can be reconstructed as detailed in Fig. 6.

As done in Equation (9), we write the efficiencies of t_1 and t_2 as follows in Equation (11):

Equation 11. Equation linking models #, $\boldsymbol{h}_1$, $\boldsymbol{h}_2$, $\boldsymbol{t}_1$ and $\boldsymbol{t}_2$

$$\varepsilon_{t1} + \varepsilon_{t2} = \frac{N_{t1}}{C_{t1}} + \frac{N_{t2}}{C_{t2}} = \frac{\varepsilon_{\#} C_{\#} + \varepsilon_{h1} C_{h1}}{C_{\#} + C_{h1}} + \frac{\varepsilon_{\#} C_{\#} + \varepsilon_{h2} C_{h2}}{C_{\#} + C_{h2}}$$

In this specific case, $C_i = m_i$ as t_1 and t_2 corresponds to a model with homogeneous relative source concentration. Then, by extracting $\varepsilon_{\#}$ and observing that $C_{\#} + C_{h2} = m_{\#} + m_{h2} = m_{t1}$, we reach Equation (12):

Equation 12. Efficiency of # depending on $\boldsymbol{h}_1$, $\boldsymbol{h}_2$, $\boldsymbol{t}_1$ and $\boldsymbol{t}_2$

$$\varepsilon_{\#} = \frac{1}{2m_{\#}} \left[\varepsilon_{t1} m_{t1} - \varepsilon_{h2} m_{h2} + \varepsilon_{t2} m_{t2} - \varepsilon_{h1} m_{h1} \right]$$

We can now calculate the efficiency of the model containing the two hotspots by inserting Equation (12) in Equation (10) leading to Equation (13):

Equation 13. Efficiency of the total model with 2 hotspots depending on #, $\boldsymbol{h}_1$, $\boldsymbol{h}_2$, $\boldsymbol{t}_1$ and $\boldsymbol{t}_2$

$$\varepsilon_{total} = \frac{\frac{R_{\#}}{2} \left[\varepsilon_{t1} m_{t1} - \varepsilon_{h2} m_{h2} + \varepsilon_{t2} m_{t2} - \varepsilon_{h1} m_{h1} \right] + \varepsilon_{h1} C_{h1} + \varepsilon_{h2} C_{h2}}{C_{\#} + C_{h1} + C_{h2}}$$

4.2.2. Generalization of theory for N hotspots

The generalization of Equation (13) can be done by augmenting the number of hotspots. The demonstration is done in three steps not further detailed in this document in the interest of better clarity for the reader.

1. Generalizing Equation (10) with N hotspots leads to Equation 14

Equation 14. Efficiency of the total model depending on # and N hotspots

$$\varepsilon_{total} = \frac{\varepsilon_{\#} R_{\#} m_{\#} + \sum_{i=1}^{N} \varepsilon_{hi} R_{hi} m_{hi}}{R_{\#} m_{\#} + \sum_{i=1}^{N} R_{hi} m_{hi}}$$

2. Generalizing Equation (12) with N hotspots leads to Equation 15

Equation 15. Efficiency of model # depending on N hotspots and $\boldsymbol{t}_i$ models

$$\varepsilon_{\#} = \frac{1}{N m_{\#}} \left[\sum_{i=1}^{N} \left(\varepsilon_{ti} m_{ti} - \sum_{\substack{j=1 \\ j \neq i}}^{N} \varepsilon_{hj} m_{hj} \right) \right]$$

3. Combination of Equation (14) and Equation (15) leads to Equation 16

Equation 16. Efficiency of the total model containing N hotspots

$$\varepsilon_{total} = \frac{\frac{R_{\#}}{N} \sum_{i=1}^{N} \left[\varepsilon_{ti} m_{ti} - \sum_{\substack{j=1 \\ j \neq i}}^{N} \varepsilon_{hj} m_{hj} \right] + \sum_{i=1}^{N} \varepsilon_{hi} R_{hi} m_{hi}}{R_{\#} m_{\#} + \sum_{i=1}^{N} R_{hi} m_{hi}}$$

The number of IUE computations required is $2N$ corresponding to each $\varepsilon_{ti}, i = 1..N$ and each $\varepsilon_{hj}, j = 1..N$.

4.2.3. Multiple hotspots relative source concentration phase space extension

When IUE produces the different hotspot models, they are all constructed with the same relative source concentration. However, a change in this concentration only implies a change in the coefficients of Equation (16) and not in the efficiency values of the models t_i and h_i calculated by ISOCS. So, an engine has been implemented in GURU to generate more models based on the already generated models. From this engine, it is possible to vary the relative source concentrations of each hotspot in each model without changing the hotspot position. The range of the relative source concentration variations is chosen by the user in GURU as well as the number of sub-models to create. Then, GURU allows constructing additional geometry models by computing the total efficiency in Equation (16) sallowing variable hotspot concentration values without further IUE/ISOCS computations. This improvement is an extension of ISOCS.

4.2.4. Validation of the hotspots combination new formalism

We performed a validation step for two purposes:

- To ensure our good understanding of what represents the $\boldsymbol{t}_i$ and $\boldsymbol{h}_i$ models;
- To validate our equations in regard with ISOCS efficiencies calculations.

Two models were generated and the only difference between them is the density of the internal material.

1. On one hand, models t_1, t_2, h_1,h_2 and **total** were generated using IUE with specific parameters. The goal was to force IUE to randomly locate the two hotspots with one common surface (Fig. 7).
2. On the other hand, with Geometry Composer, we calculated activities of all the models #, t_1, t_2, h_1,h_2 and **total** without using IUE, but considering the parameters from point 1. described above and extracted from the UGS file.

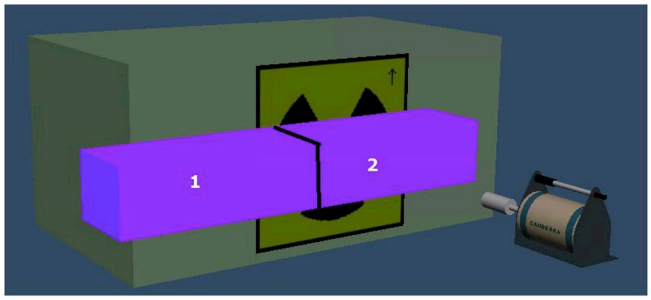

Fig. 7. Representation of two hotspots in Geometry Composer by cutting one large hotspot in two smaller hotspots.

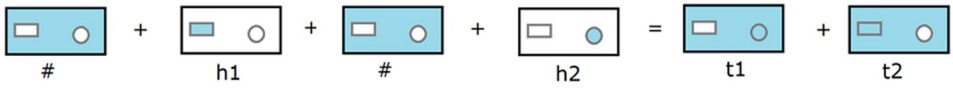

Fig. 6. Combination of models # and $\boldsymbol{h}_1$ and $\boldsymbol{h}_2$ to get $\boldsymbol{t}_1$ and.$\boldsymbol{t}_2$

In order to be able to model two hotspots in Geometry Composer we used a trick: the two hotspots are touching each other and with the same dimension (hotspots 1 and 2 in Fig. 7). The total dimension of the hotspot is $124 \times 40 \times 50$ cm^3 with a source relative concentration 10 times higher than the box. The dimension of the box is $250 \times 115 \times 137$ cm^3. The distance source-detector is 125 cm. The detector model used for this simulation is a CANBERRA GC4018. It is a coaxial p-type high purity germanium detector with 40% relative efficiency. This allowed us to generate two hotspots in Geometry Composer while only one can be modelled with a complex box.

Results obtained from these two similar methods of efficiency calculations are summarized in Table 1 for the low and high density material models. "IUE" refers to point 1 and "Manual" refers to point 2 in the table. Then "Rel. Dif." refers to the relative difference calculated between IUE and Manual methods.

The first interesting results is that our understanding of t_1, t_2, h_1, h_2 is correct as, for all the calculations, IUE and Manual methods give the same result with less than 0.01% of relative difference. The difference only comes from the digits numbers considered, given in the. ECC (5 digits) and the. UEC (4 digits).

Another interesting result concerns the calculation of # with Equation (12). "# ISOCS" in Table 1 refers to the efficiency of # model computed with Geometry Composer whereas "# new method" has been built from Equation (12). In all the cases, the efficiencies found are similar with less than 0.15% of difference between ISOCS calculation and reconstruction from Equation (12).

Finally, comparison of the total model efficiency shows discrepancies in some particular cases. Comparing IUE reconstruction with ISOCS reconstruction shows a discrepancy of 1% at low density and 7.4% at high density. However, our reconstruction with equations of this section compared to ISOCS total model shows excellent agreement with less than 0.3% of differences in both cases.

As a conclusion, results reconstructed with our new formalism and calculated with ISOCS show very good agreements. However, results on total model reconstructed with IUE show differences for high density materials with ISOCS model. A detailed investigation of this effect is ongoing and at the present stage of writing, a software bug, pending correction, cannot be fully excluded.

Different energies (from 45 keV to 3 MeV) have been tested as well as models with four hotspots leading to similar results and conclusions.

Table 1
Comparison between the full energy peak efficiencies calculated by IUE and reconstruction of each model total, #, h_1, h_2, t_1 and t_2 with geometry composer efficiencies at 100 keV.

	Low density materials, air (0.00129 g/cm^3)			High density materials, Steel 304 (7.8 g/cm^3)		
	IUE	Manual	Rel. Dif.	IUE	Manual	Rel. Dif.
h2	5.31E-05	5.31E-05	<0.01%	5.28E-26	5.28E-26	0.01%
t2	4.30E-05	4.30E-05	<0.01%	2.24E-07	2.24E-07	<0.01%
h1	5.33E-05	5.33E-05	<0.01%	5.39E-26	5.39E-26	<0.01%
t1	4.30E-05	4.30E-05	<0.01%	2.24E-07	2.24E-07	<0.01%
# ISOCS	–	4.22E-05	–	–	2.41E-07	–
# New method	4.22E-05	4.22E-05	<0.01%	2.41E-07	2.41E-07	<0.01%
Total sample ISOCS	4.92E-05	4.87E-05	−0.95%	8.90E-08	9.56E-08	7.41%
Total sample new method	4.88E-05	4.88E-05	<0.01%	9.59E-08	9.59E-08	<0.01%

4.2.5. Discussion

The formalism developed in this paper applies to all cases with a homogeneous matrix including one or multiple hotspots in a box type geometry. It addresses heterogeneous activity distributions and the presence of attenuating material (matrix) in the container/measurement sample. It also addresses the variations in geometry such as the sample dimensions, the source to detector distance, the material types and the densities. The attenuation effects due to the presence of a matrix within the container is achieved via the ISOCS calculations that are performed for each individual geometry (paragraph 3.2, Figs. 5 and 6).

The relative source concentration in ISOCS allows defining the radioactive nature of each element within the container (hotspot or just an attenuation material). In other words, an attenuation material has a relative source concentration of 0. Note that we started from the first physics principles defining the full peak efficiency of a given gamma line as defined in Equation (8). The efficiency is simply derived from the ratio of the number of photons registered in the peak by the number of photons emitted by the source.

5. Experimental setup

In order to validate the efficiency of the method, we studied three experimental cases. We measured an empty container with radioactive sources inside, for which positions and activities are well known. Three experiments are performed with different purposes (description in appendix 2):

- **Case 1** has the purpose to reconstruct the real expected activity of one hotspot simulated by a source of mixed radionuclides: Co-60, Am-241 and Cs-137. The experiment was performed with two detectors located on the lateral faces of the container (Table 2).

- **Case 2** has the purpose to reconstruct the real expected activity inside the container taking into account three hotspots, each formed by a mix of Co-60, Am-241 and Cs-137, in order to construct sources with similar radionuclide types but different activity distributions. Hence, each location would contain Co-60, Am-241 and Cs-137 sources. The experiment was done with four detectors on each of the accessible faces of the container (Table 3).

- **Case 3** was done to reconstruct the real activity inside the container taking into account three different hotspots, each one simulated by different radionuclides: Co-60, Am-241 and Cs-137. The experiment was done with two detectors located on the lateral faces of the container (Table 4).

The configuration of the experiment is detailed in Figs. 8 and 15. The container is a standard container made of iron with a thickness of 1.5 mm. Sources are located in tin cans with 0.3 mm thickness. As the tin cans are not simulated in ISOCS we corrected the activity by calculating an apparent activity for Am-241 taking into account the attenuation due to these cans. It was necessary to only correct Am-241 activity due to the low energy of its gamma rays. The sources have been selected in order to have a representation of the energy range of the detector, from 60 keV to 1.33 MeV.

Table 2
Hotspot description in case-study 1.

Case 1		
Hotspot number	RN	Activity (kBq)
S1.1	Co-60	32
	Am-241	9
	Cs-137	276

Table 3
Hotspot description in case-study 2.

Case 2		
Hotspot number	RN	Activity (kBq)
S2.1	Co-60	32
	Am-241	9
	Cs-137	276
S2.2	Co-60	33
	Am-241	9
	Cs-137	95
S2.3	Co-60	54
	Am-241	94
	Cs-137	54
Total	Co-60	119
	Am-241	112
	Cs-137	425

Table 4
Hotspot description in case-study 3.

Case 3		
Hotspot number	RN	Activity (kBq)
S3.1	Co-60	32
S3.2	Am-241	9
S3.3	Cs-137	276

The first results of optimization have given discrepancies (factor of 2 compared to the real activity) on two Cs-137 sources which were located in a brass source-holder. We observed that these sources were not isotropic and consequently we performed the following corrections:

- For each measurement, we turned the source in the direction of the detector in order to avoid the anisotropy,
- We calculated an apparent activity by gamma-spectroscopy of the two Cs-137 sources to avoid the attenuation of the source-holder.

For each experiment and for each detector we calculated the efficiency uncertainties due to the presence of hotspots (position, dimension and relative source concentration) with the method detailed in paragraph 2. Then, the uncertainties are reduced by optimizing spectroscopy measurements using the methodology described in paragraph 3. Finally, the new uncertainty and average values are extracted considering the 10 best-estimate models as possible models.

6. Results of quantification and optimization of uncertainties

In the next, we denote as:

- Count uncertainty, the uncertainty coming from the spectroscopy report (peak area, gamma emission intensity, numerical approximations);
- Model uncertainty, the uncertainty coming from the geometric model description (dimensions, hotspots, activity distribution);
- Standard deviation of the mean between measurements, the standard deviation of the mean computed considering spectroscopy results originating from different detectors.

6.1. Case 1: hotspot with mixed radionuclides

The purpose here is to study the possibility of reconstructing the real activities in a simple case with only one hotspot. F.

6.1.1. Uncertainty quantification

In Fig. 9, the light-brown part shows the variation range of the relative difference of efficiency curves generated by IUE compared to the one determined for the reference model (no hotspot, homogeneous activity concentration). The red curve is the mean curve over the light-brown part. It shows a bias of −25%. This indicates that in the case where the geometry is not well known, the uniform distribution models commonly used presents activities that are underestimated by 25%.The standard deviation at 1 σ (orange envelop) is of around 30%. This value represents in the next the uncertainty due to the model geometry. The gamma-spectroscopy results before optimization are described in Table 5.

6.1.2. Uncertainty reduction and best models optimization

The optimization of gamma spectroscopy results is performed. We calculate the average value of activity for each radionuclides over the ten best-estimate models as well as the corresponding model uncertainty (standard deviation of the mean of the 10 best models). The results are presented in Table 6. We observe that for each detector, the new model

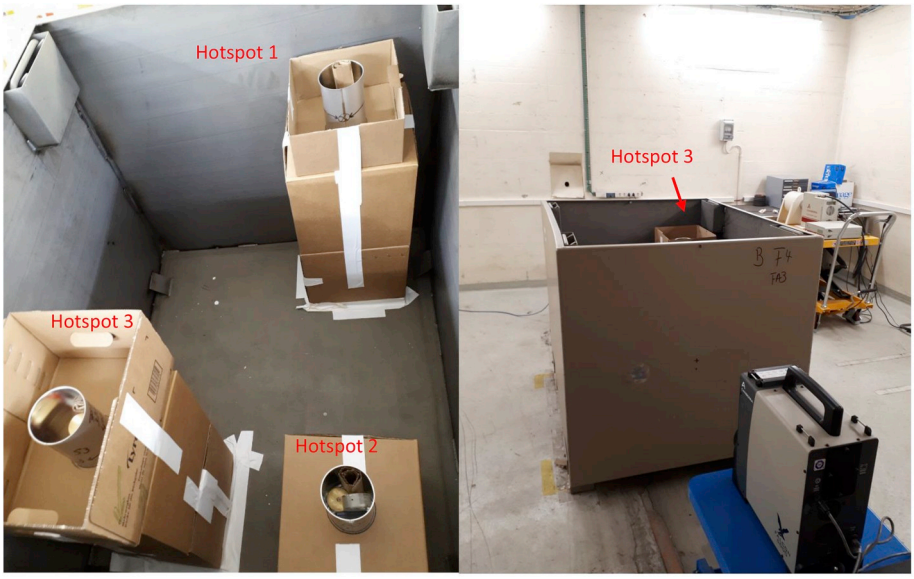

Fig. 8. Description of one of the experiment configuration. Left picture: inside the container, sources are located in tin cans. Right pictures, measurement configuration with FALCON detector.

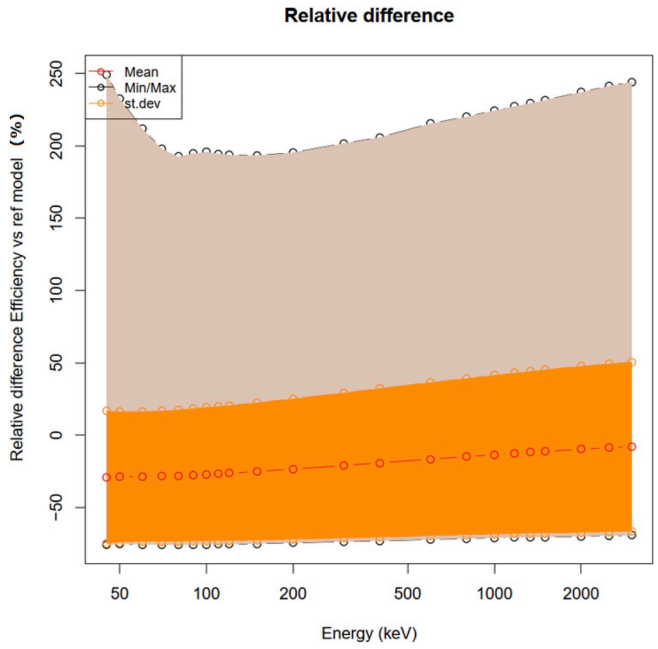

Fig. 9. Relative efficiency variation over energy compared to the reference model with homogeneous activity concentration.

uncertainty has been largely reduced. We recall that, prior to the optimization, the standard deviation is ~30% and the bias is ~25%. The measured activity, after optimization is more consistent compared to the expected value.

Table 7 shows comparisons between average activities over all detectors and associated standard deviation of the mean between the measurements before and after optimization. The activity measured before optimization shows a difference of approximatively the calculated bias (25%). The new standard deviation of the mean after optimization is largely reduced showing that the two detectors get similar activity values.

In Fig. 10, we can observe that for each radionuclides, the model's uncertainties have been largely reduced except for Am-241. For Cs-137 and Co-60, uncertainties have been lowered by a factor of 6. The activity results from both detectors 1 and 2 are coherent and in line with the expected source activity.

To illustrate the optimization process, each model's activity of Cs-137 is calculated and plotted for both detector in Fig. 11 (sorted decreasing for the detector number 2 and plotted with the corresponding activity value of detector number 1). We observe that both red and blue curves for detector 1 and 2 cross each other. The best-estimate model is the one which minimizes the "distances" between these two curves.

6.2. *Case 2: three hotspots with homogeneous distribution of radionuclides*

The purpose of this experiment is to study the possibility of reconstructing the expected activities when more than one hotspot exist in a sample.

6.2.1. *Uncertainty quantification*

In all the three cases presented in this work, we find that the uncertainty distribution shown in Fig. 9 is the same. Activities using the homogeneous model for case 2 are summarized in Table 8. We show that, compared to the expected activities, the results of a homogenous model can lead to underestimation of the average activity computed over the 4 detectors (detectors 1, 2 and 4 measured activities of Co-60 below the expected value, for example). The reference model activity presents a bias of 25% and a standard deviation of 30%.

6.2.2. *Uncertainty reduction*

The optimization of spectroscopy results is performed. We calculate the average value of activity for each radionuclides over the 10 best-estimate models as well as the corresponding model uncertainty. The results are presented in Table 9. Activity values have been increased compared to the values from homogeneous model. They are now closer to the expected value and the model uncertainty has also been reduced.

We observe that Co-60 and Cs-137 perfectly fit with the expected value of the sources activities (Table 10). Moreover, the standard

Table 5
Spectroscopy results with homogeneous activity model used, before optimization. Case 1.

Radionuclide	Activity Det. 1 (kBq)	Count Unc. Det. 1 (2σ)	Activity Det. 2 (kBq)	Count Unc. Det. 2 (2σ)	Expected Hotspot certified Activity (kBq)	Hotspot activity uncertainty (% at 2σ)
Co-60	41.1	10%	14.8	10%	32	3%
Cs-137	320	16%	119	16%	276	25%
Am-241	8.39	25%	3.7	28%	9	10%

Table 6
New activities after the optimization of the spectroscopy results, compared to real source activity. Case 1.

Radionuclide	Activity Det. 1 (kBq)	Count Unc. Det. 1 (2σ)	Model Unc. Det. 1 (2σ)	Activity Det. 2 (kBq)	Count Unc. Det. 2 (2σ)	Model Unc. Det. 2 (2σ)	Expected Hotspot certified Activity (kBq)	Hotspot activity uncertainty (% at 2σ)
Co-60	33.3	10%	2%	33.4	10%	2%	32	3%
Cs-137	281	16%	3%	281	16%	3%	276	25%
Am-241	9.52	25%	9%	9.59	28%	9%	9	10%

Table 7
Comparison of activities and standard deviation of the mean between measurement before and after optimization. Case 1.

Radionuclide	Before Optimization		After Optimization			
	Average activity (kBq)	Std. deviation of the mean	Average activity (kBq)	Std deviation of the mean	Expected Hotspot certified Activity (kBq)	Hotspot activity uncertainty (% at 2σ)
Co-60	28.0	47%	33.4	<1%	32	3%
Cs-137	219.5	46%	281.0	<1%	276	25%
Am-241	6.0	39%	9.6	<1%	9	10%

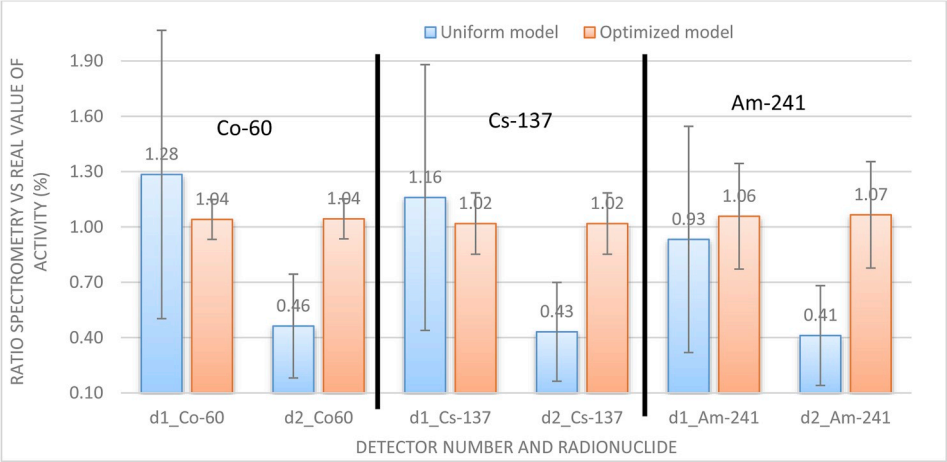

Fig. 10. Comparisons of ratio with real value of activity for uniform and optimized models. The uncertainties displayed on the bar chart represent the quadratic sum of those from GENIE2000 and GURU analysis at 2σ.

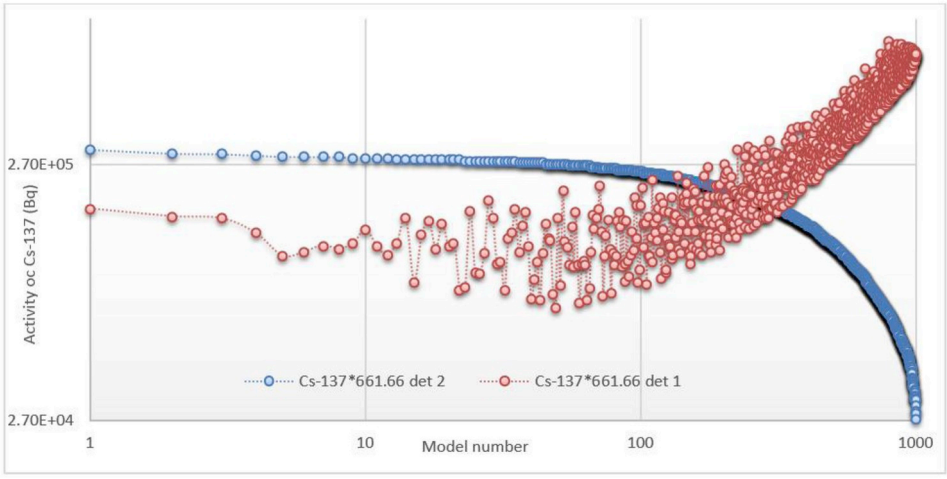

Fig. 11. Activities calculated for each model sorted with decreasing activity for detector 2.

Table 8
Spectroscopy results with homogeneous activity inside the container, before optimization. Case 2.

Radionuclide	Activity Det. 1 (kBq)	Count Unc. Det. 1 (2σ)	Activity Det. 2 (kBq)	Count Unc. Det. 2 (2σ)	Source certified Activity (kBq)	Source activity uncertainty (% at 2σ)
Co-60	96.8	10%	99.3	10%	119	3%
Cs-137	255	16%	414	16%	425	13%
Am-241	68.20	24%	53.8	24%	112	5%
Radionuclide	**Activity Det. 3 (kBq)**	**Count Unc. Det. 3 (2σ)**	**Activity Det. 4 (kBq)**	**Count Unc. Det. 4 (2σ)**	**Source certified Activity (kBq)**	**Source activity uncertainty (% at 2σ)**
Co-60	131	10%	81.5	10%	119	3%
Cs-137	302	16%	489	16%	425	13%
Am-241	78.80	24%	44.9	24%	112	5%

deviation of the mean between the 4 measurements have been largely reduced to reach a value below 1%. For Am-241, the activities agree within 20% after optimization, between expected value and measured value (45% before optimization). Note that for Am-241, the intrinsic GENIE2000 uncertainties (detector's uncertainties) of the reference spectroscopy measurement is 24% at 2σ. The results are summarized in Fig. 12.

6.3. Case 3: three hotspots with heterogeneous distribution of radionuclides

The purpose of this experiment is to study the possibility of reconstructing the expected activities when exist in the container heterogeneities concerning the radionuclides types.

6.3.1. Uncertainty quantification

The uncertainty distribution shown in Fig. 9 is the same for case 3 than for the previous cases. Activities using the homogeneous model are

Table 9
New activities after optimizing the spectrometry reports, compared to real source activity. Case 2.

Radionuclide	Activity Det. 1 (kBq)	Count Unc. Det. 1 (2σ)	Model Unc. Det. 1 (2σ)	Activity Det. 2 (kBq)	Count Unc. Det. 2 (2σ)	Model Unc. Det. 2 (2σ)	Source certified Activity (kBq)	Source activity uncertainty (% at 2σ)
Co-60	119.8	10%	1.2%	120.6	10%	1.3%	119	3%
Cs-137	407	16%	1.9%	422	16%	2.2%	425	13%
Am-241	88.70	24%	3.7%	87.2	24%	3.7%	112	5%
Radionuclide	**Activity Det. 3 (kBq)**	**Count Unc. Det. 3 (2σ)**	**Model Unc. Det. 3 (2σ)**	**Activity Det. 4 (kBq)**	**Count Unc. Det. 4 (2σ)**	**Model Unc. Det. 4 (2σ)**	**Source certified Activity (kBq)**	**Source activity uncertainty (% at 2σ)**
Co-60	120.3	10%	1.1%	120.2	10.00%	1.1%	119	3%
Cs-137	421	16%	2.1%	414	16.20%	2.7%	425	13%
Am-241	88.80	24%	3.8%	88.8	24.50%	3.8%	112	5%

Table 10
Comparison of activities and standard deviation of the mean between measurement before and after optimization. Case 2.

Radionuclide	Before optimization		After optimization			
	Average activity (kBq)	Std deviation of the mean	Average activity (kBq)	Std deviation of the mean	Source certified Activity (kBq)	Source activity uncertainty (% at 2σ)
Co-60	102.2	10%	120.2	<1%	119	3%
Cs-137	365.0	14%	416.0	1%	425	13%
Am-241	61.4	12%	88.4	<1%	112	5%

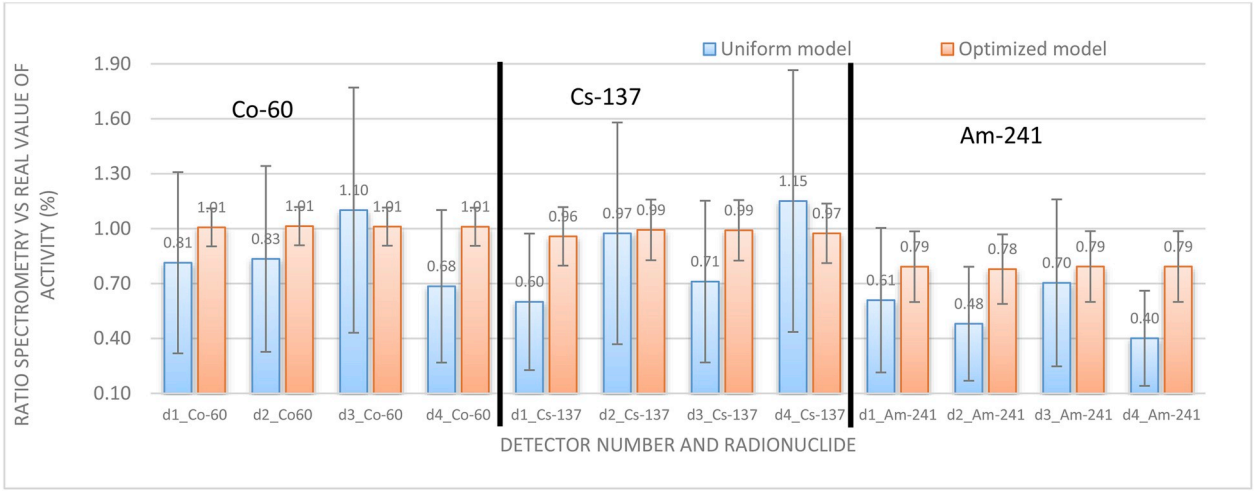

Fig. 12. Comparisons of ratio with real value of activity for uniform and optimized models. The uncertainties displayed on the bar chart represent the quadratic sum of those from GENIE2000 and GURU analysis at 2σ.

Table 11
Spectroscopy results with homogeneous activity inside the container, before optimization.

Radionuclide	Activity Det. 1 (kBq)	Count Unc. Det. 1 (2σ)	Activity Det. 2 (kBq)	Count Unc. Det. 2 (2σ)	Source certified Activity (kBq)	Source activity uncertainty (% at 2σ)
Co-60	11.6	12%	41.1	10%	32	3%
Cs-137	469.0	16%	90.9	16%	276	25%
Am-241	3.2	93%	13.9	26%	9	10%

Table 12
New activities after optimizing the spectroscopy reports, compared to real source activity.

Radionuclide	Activity Det. 1 (kBq)	Count Unc. Det. 1 (2σ)	Model Unc. Det. 1 (2σ)	Activity Det. 2 (kBq)	Unc. Det. 2 (2σ)	Unc. Model (2σ)	Source certified Activity (kBq)	Source activity uncertainty (% at 2σ)
Co-60	27.9	12%	1.9%	27.9	10%	3.1%	32	3%
Cs-137	237.4	16%	2.0%	283.4	16%	1.7%	276	25%
Am-241	10.2	94%	1.9%	8.8	26%	1.9%	9	10%

Table 13
Comparison of activities and standard deviation of the mean between measurements before and after optimization. Case 3.

Radionuclide	Before optimization		After optimization			
	Average activity (kBq)	Std deviation of the mean	Average activity (kBq)	Std deviation of the mean	Source certified Activity (kBq)	Source activity uncertainty (% at 2σ)
Co-60	26.4	56%	27.9	<1%	32	3%
Cs-137	280.0	68%	260.4	9%	276	25%
Am-241	8.6	63%	9.5	8%	9	10%

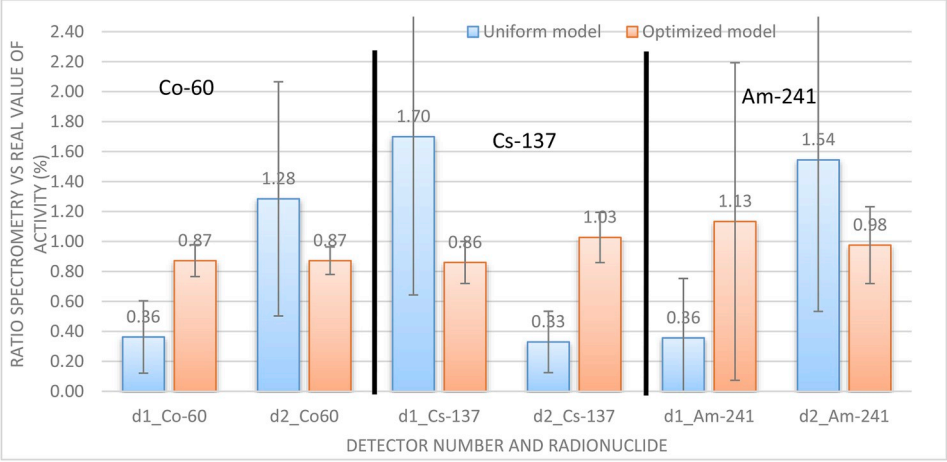

Fig. 13. Comparisons of ratio with real value of activity for uniform and optimized models. The uncertainties displayed on the bar chart represent the quadratic sum of those from GENIE2000 and GURU analysis at 2σ.

summarized in Table 11. A large uncertainty is found regarding detector 1 for Am-241 because this detector is located far from the americium source and consequently, the count rate is low. The reference model activity presents a bias of 25% and a standard deviation of 30%.

6.3.2. Uncertainty reduction

The optimization process is performed on each detector for each radionuclide. We calculate the average value of activity for each radionuclide over the 10 best-estimate models as well as the corresponding uncertainty. The results are presented in Table 12.

As observed in the previous experiments, the standard deviation of the mean between both detectors is reduced after optimization (Table 13). In addition, the actual activity value has changed as well and the results show again good agreements with the expected value. The results are summarized in Fig. 13.

7. Conclusions

We have developed a theory that allows for the qualification of gamma-spectroscopy geometry models. A software tool has been created:

- To quantify the impact of geometry uncertainties on the efficiency curves and consequently on the specific activity results,
- To optimize these uncertainties and re-estimate a new activity more consistent with the reality, by performing multiple gamma spectroscopies on a material.

The challenge is linked to the generation of multiple hotspots for which IUE needs to perform numerous calculations and recombination of the associated efficiencies. This formalism has been reproduced in order to be able to study the impact of hotspots on the efficiency uncertainty.

A first validation of hotspot treatment has been performed to ensure the quality of the method by comparisons with different approaches from ISOCS/LabSOCS. The results were found to be consistent.

We have shown the reliability of the method for three different applications with different particularities, regarding the heterogeneous distribution of the activity concentrations.

The quantification of uncertainties has shown that a bias of 25% exists in this specific case, leading to an underestimation of activities of 25% by gamma-spectroscopy measurements with uniform source distribution. After optimization, the activity values have been corrected from this bias by the GURU tool.

Moreover, the model's standard deviation of the mean before optimization between two detector measurements can be quite high as we found a maximum of 68%. However, after optimization, this value is strongly reduced and the maximum was only about 9%, showing a considerable reduction of the uncertainty by a factor 8.

The results are very encouraging as the real source activity has been better estimated after optimization. A distribution of the tool to external interested parties can be envisaged.

APPENDIX 1. SEQUENTIAL PROCESS FOR THE USE OF GURU

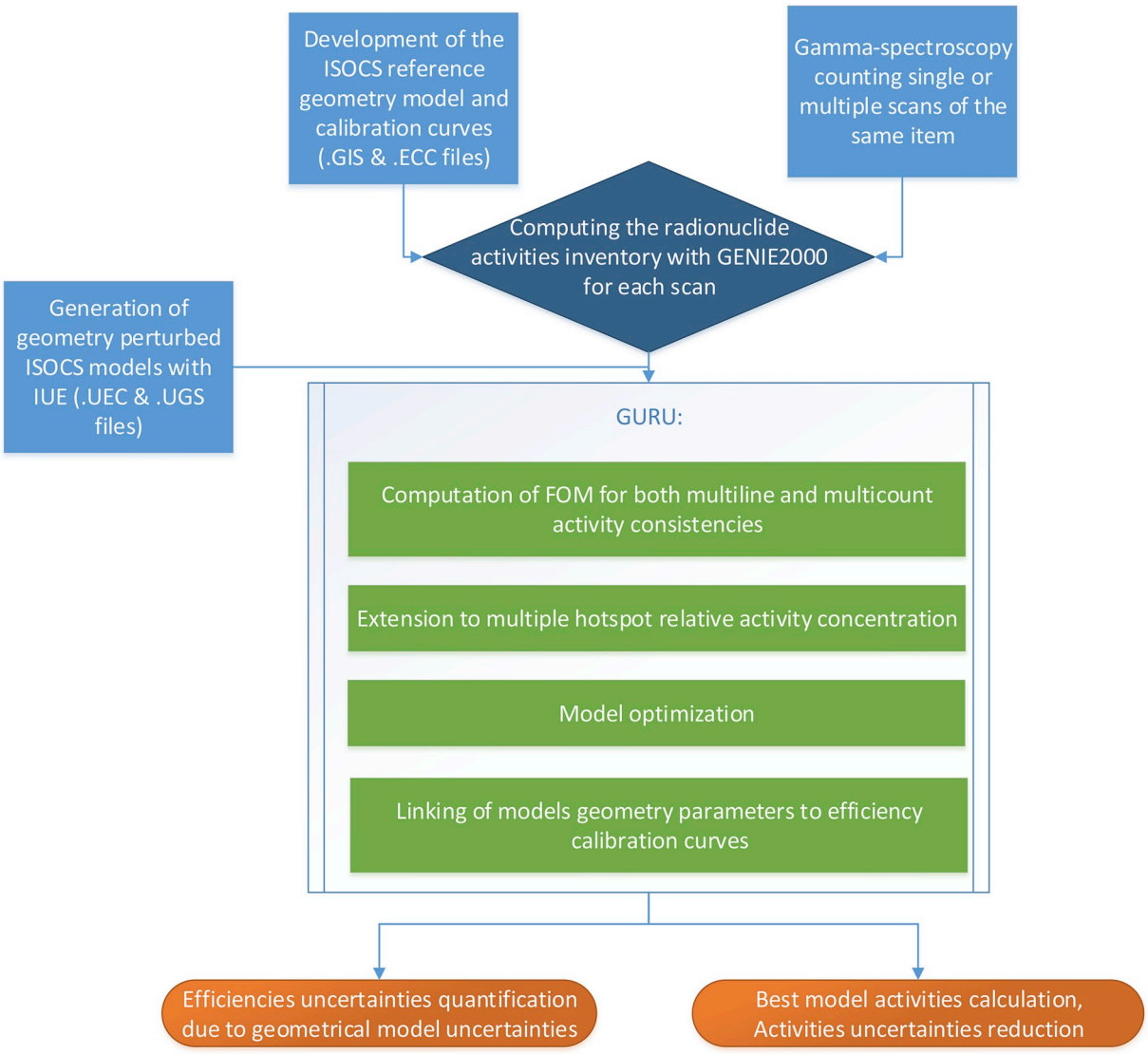

Fig. 14. Sequential process for the use of GURU .

APPENDIX 2. DESCRIPTION OF EXPERIMENTAL VALIDATION CASES

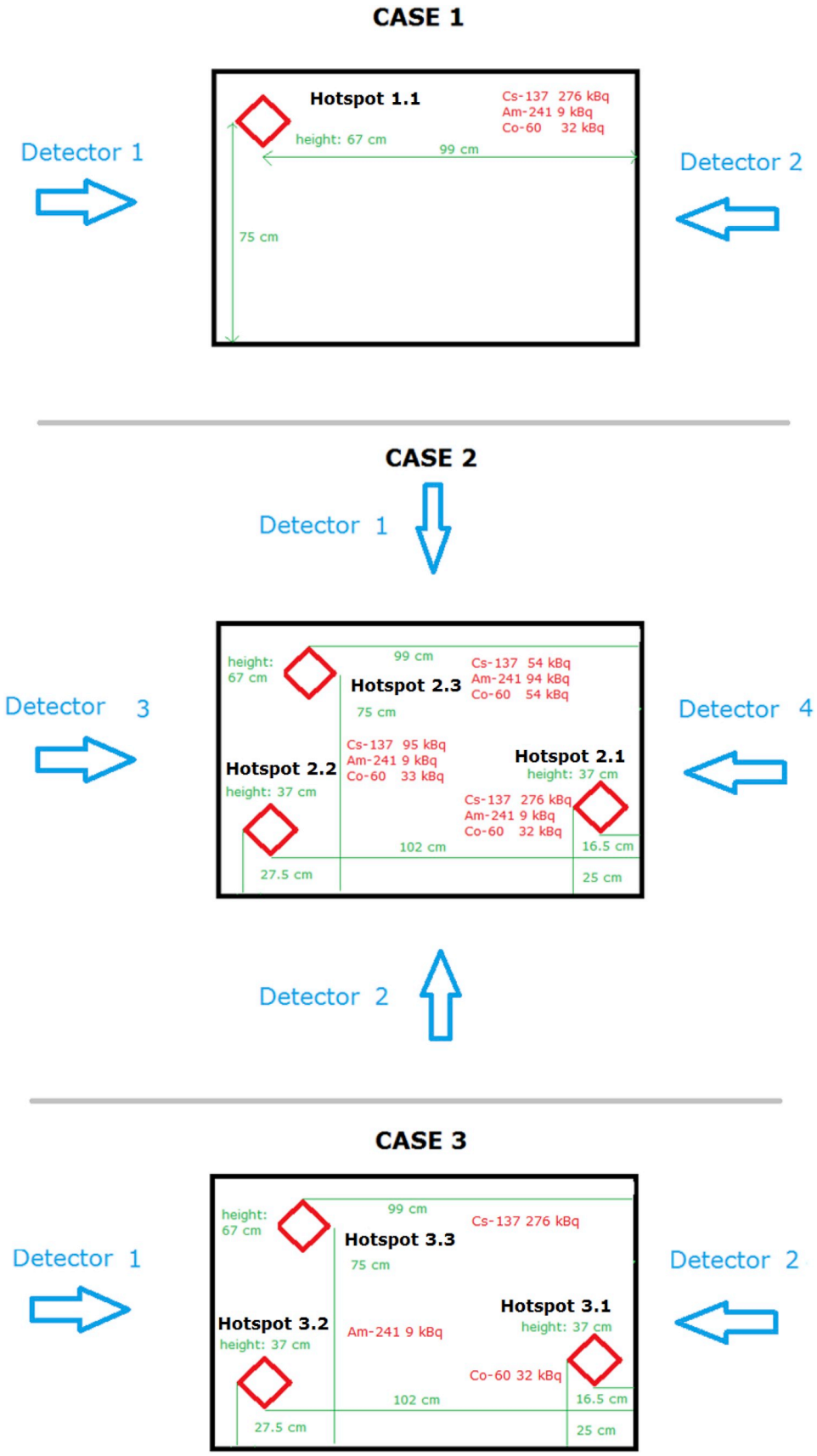

Fig. 15. Diagram of the validation measurement configurations

References

Belgya, T., May 2014. Uncertainty calculation of functions of γ-ray detector efficiency and its usage in comparator experiments. J. Radioanal. Nucl. Chem. 300.

Bosko, A., Menaa, N., Spillane, T., Bronson, F., Venkataraman, R., Russ, W.R., Mueller, W., Nizhnik, V., 2011. Efficiency optimization employing random and smart search using multiple counts and line activity consistency benchmarks. In: Proceedings of WM2011 Conference, February 27-March 3 (Phoenix, AZ).

Bronson, F., October 1997. ISOCS, a laboratory quality Ge gamma spectroscopy system you can take to the source for immediate high quality results. In: Proceedings of the Rapid Radioactivity Measurements in Emergency and Routine Situations Conference. UK.

Bronson, F., Young, B.M., Atrashkevich, V., June 1997. ISOCS mathematical calibration software for germanium gamma spectroscopy of small and large objects. In: Transactions of the American Nuclear Society Annual Meeting.

Bronson, F., et al., 2008. Probabilistic uncertainty estimator for gamma-spectroscopy measurements. J. Radioanal. Nucl. Chem. 276 (No.3), 589–594.

Ceccatelli, A., et al., March 2017. Calculation spreadsheet for uncertainty estimation of measurement results in gamma-ray spectrometry and its validation for quality assurance purpose. Appl. Radiat. Isot. 124, 7–15.

GUM, Evaluation of Measurement Data, 2008. Supplement 1 of the Guide to the Expression of Uncertainty in Measurement. JCGM101. September 2008.

GUM, Evaluation of Measurement Data, 2008. Guide to the Expression of Uncertainty in Measurement. JCGM100. September 2008.

Ilie, G., et al., 2013. Gamma spectroscopy with automated efficiency optimization for nuclear safeguards applications. In: 3rd International Conference on Advancements in Nuclear Instrumentation. Measurement Methods and Their Applications.

Kaminski, S., Jakobim, A., Wilhelm, Chr, 2014. Uncertainty of gamma-ray spectrometry measurement of environmental samples due to uncertainties in matrix composition, density and sample geometry. Appl. Radiat. Isot. 94, 306–313.

Menaa, N., et al., 2011. Mathematical efficiency calibration with uncertain source geometries using smart optimization. In: 2nd International Conference on Advancements in Nuclear Instrumentation, Measurement Methods and Their Applications.

Nakazawa, D., et al., 2010. The efficiency calibration of non-destructive gamma assay systems using semi-analytical mathematical approaches – 10497. In: WM2010 Conference, March 7-11 (Phoenix, AZ).

Sima, O., 2017. Efficiency computation for gamma-ray spectrometry assessment of samples with intrinsic inhomogeneity. Appl. Radiat. Isot. 126, 146–149.

Sima, O., 2018. On homogeneity approximation in calibration of gamma-spectrometry assessment of bulk samples. Appl. Radiat. Isot. 134, 137–141.

Spillane, T., Menaa, N., Atrashkevich, V., Bosko, A., Bronson, F., Nakazawa, D., Russ, W. R., Venkataraman, R., August 2010. An adaptive approach to mathematical efficiency calibration with uncertain source geometries. In: Proceedings of the American Nuclear Society Topical Meeting on Decommissioning, Decontamination and Reutilization. Idaho Falls, ID USA.

Venkataraman, R., Bronson, F., Atrashkevich, V., Young, B., Field, M., 1999. Validation of in Situ Object counting system (ISOCS) mathematical efficiency calibration software. Nucl. Instrum. Methods 422, pp450–454.

Venkataraman, R., Bronson, F., Atrashkevich, V., Field, M., Young, B.M., 2003. Improved detector response characterization method in ISOCS and LabSOCS. In: Methods and Applications of Radioanalytical Chemistry (MARC VI) Conference.

Venkataraman, R., Croft, S., Villani, M., McElroy, R.D., Estep, R.J., 2005. Total Measurement Uncertainty Estimation For Tomographic Gamma Scanner. In: Proceedings of 46th Annual Meeting of the INMM (Institute of Nuclear Materials Management), Phoenix, Arizona, USA.

Zhang, W., et al., March 2017. Design an optimization of a dual-HPGe gamma spectrometer and its cosmic veto system. IEEE Trans. Nucl. Sci. 64 (3).